IOP Publishing and International Atomic Energy Agency Nuclear Fusion

Nucl. Fusion **48** (2008) 024017 (9pp) doi:10.1088/0029-5515/48/2/024017

On the accuracy of some mapping techniques used to study the magnetic field dynamics in tokamaks

D. Constantinescu[1], **O. Dumbrajs**[2,3], **V. Igochine**[4] **and B. Weyssow**[5]

[1] Department of Applied Mathematics, University of Craiova, A.I.Cuza Street 13, Craiova 1100, (200585) Romania[a]
[2] Helsinki University of Technology, Association Euratom-Tekes, PO Box 2200, FIN-02015 HUT, Finland
[3] Institute of Solid State Physics, Association Euratom-University of Latvia, Kengaraga Street 8, LV-1063, Riga, Latvia
[4] MPI für Plasmaphysik, Euratom-Association, D-85748 Garching, Germany
[5] Statistical and Plasma Physics, Université Libre de Bruxelles, CP 231, Boulevard du Triomphe, 1050 Bruxelles, Belgium[b]

Received 4 June 2007, accepted for publication 4 September 2007
Published 30 January 2008
Online at stacks.iop.org/NF/48/024017

Abstract
The dynamics of magnetic field lines and of charged particles in toroidal chambers are commonly analysed by numerically solving the dynamical equations. They may also be analysed using deterministic reduced models, i.e. low-dimensional discrete time approximations (maps) of the Hamiltonian continuous time models. We report on the accuracy of the latter method by considering the mapping technique derived from the Hamilton–Jacobi equation. The optimum time stepping in some models for the study of the magnetic field in tokamaks is determined by using local criteria. Special attention is given to the analysis of stochasticity produced by time discretization.

PACS numbers: 52.25.Gj, 05.45.Gg, 05.45.Pq

(Some figures in this article are in colour only in the electronic version)

1. Introduction

In tokamaks charged particles are confined by a magnetic field obtained by the superposition of two basic components acting in the direction of the major, respectively, minor curvatures of the torus. It is well known that the magnetic field lines can be regarded as trajectories of a Hamiltonian system obtained from the equations of the magnetic field by using the Clebsh representation [1]. The Hamiltonian of the system is the poloidal magnetic flux and the symplecticity of the Hamiltonian system is the geometrical expression of the magnetic flux conservation property contained in the equations of the magnetic field.

The initial equations and the Hamiltonian system describe the three-dimensional configuration of the magnetic field. Because sometimes it is difficult to understand and to interpret complex three-dimensional structures, a two-dimensional visualization is useful. The reduction of one dimension can be obtained using the Poincaré map: instead of studying the motion of the magnetic field line around the torus, successive intersections of the magnetic field line with the fixed poloidal section can be considered in order to describe its dynamics.

The first application of a Hamiltonian map to the study of the magnetic field in a tokamak (in the presence of a magnetic limiter) appears to be that done by Martin and Taylor in 1984 [2]. Later many mapping models were proposed for the study of various magnetic configurations (only some 'historical' papers are mentioned here): in 1987 a global model for a specific stellarator (W VII-A) was introduced by Wobig [3], some models of the edge region (scrape-off layer) of a tokamak were studied by Punjabi *et al* [4] by means of a simple algebraic map and by Abdullaev and Zaslavski [5] using the 'separatrix map', a model compatible with the toroidal geometry was proposed by Balescu *et al* [6], some reversed shear magnetic configurations were studied by Davidson *et al* [7], Oda and Caldas [8], Balescu [9], etc.

For an accurate description of the magnetic field the mapping model must be closely related to the Hamiltonian

[a] Association Euratom-Mec, Romania.
[b] Euratom-Belgian State Association for Fusion.

system. It can be obtained in two philosophically different ways: (i) by numerical integration (using appropriate methods, namely, symplectic integrators) with small steps and (ii) by the mapping technique that uses large steps. The latter is a modern technique providing important advantages: the computational time needed to obtain the phase portrait is several orders smaller than for the numerical integration and (which is more important) it has better accuracy in the study of chaotic dynamics, due to the fact that the accumulation of the round-off errors is reduced.

Rigorous methods for obtaining discrete models were presented in [10,11]. The recent and excellent monograph [12] is a systematic study of the mapping techniques and of their applications.

The mapping technique we focus on in this paper, derived from the Hamilton–Jacobi method, was proposed in [10] by Abdullaev. In that paper the author also analysed the accuracy of the symmetric map by comparing the mapping results with the results obtained by means of the symplectic integration using numerical methods. From the analysed examples it was found that the maps with the time step comparable to the perturbation period have the same accuracy as the symplectic integrators with the integration step two or three orders smaller. Hence mapping is a powerful tool for discretization of the Hamiltonian system.

It is obvious that by choosing smaller steps in the symmetric map one obtains results closer to the continuous case, but we are interested in optimizing the computational time; hence, an important problem is to choose the largest possible mapping step for which the main properties of the continuous system are preserved.

The paper is organized as follows: in section 2 some basic considerations of the Hamiltonian description of the magnetic field lines and of the mapping technique based on the Hamilton–Jacobi method are presented; section 3 is devoted to the criteria used for measuring the accuracy of a map; these criteria are applied in section 4 for determining the optimal mapping step in the three models used for the description of the magnetic field lines in tokamaks; a summary and conclusions are given in section 5.

2. Basic results

Because tokamaks are toroidal devices it is natural to use the toroidal coordinates (r, θ, ζ) in order to describe the configuration of the magnetic field (ζ is the toroidal angle and (r, θ) are the polar coordinates in a circular poloidal cross-section having the radius a), due to the specific form of the device.

The magnetic field $\vec{B}$ with the toroidal flux $\psi = \psi(r, \theta, \zeta)$ is constrained to obey the conditions

$$\nabla \cdot \vec{B} = 0 \qquad \vec{B} \cdot \nabla\psi = 0. \tag{1}$$

From the Clebsh representation ($\vec{B} = \nabla\psi \times \nabla\theta + \nabla\zeta \times \nabla H$) the Hamiltonian system is obtained

$$\frac{\mathrm{d}\psi}{\mathrm{d}\zeta} = -\frac{\partial H}{\partial\theta} \qquad \frac{\mathrm{d}\theta}{\mathrm{d}\zeta} = \frac{\partial H}{\partial\psi}, \tag{2}$$

which describes the magnetic field configuration. For a circular plasma section the toroidal flux ψ is related to the poloidal radius by $\psi = r^2/(2a^2)$. In this formalism (ψ, θ) appear as a pair of canonical variables. The Hamiltonian of the system is the poloidal magnetic flux $H = H(\psi, \theta, \zeta) = H_0(\psi) + H_1(\psi, \theta, \zeta)$, which can be expressed as a sum of the unperturbed flux $H_0(\psi) = \int \mathrm{d}\psi/q(\psi)$ (here $q = q(\psi)$ is the safety factor) and of the perturbation

$$H_1(\psi, \theta, \zeta) = \sum_{m,n} H_{mn}(\psi)\cos(m\theta - n\zeta + \chi_{mn}). \tag{3}$$

The variable ζ is interpreted as the 'time' variable, so that the Hamiltonian equations for the magnetic field lines are interpreted as 'equations of motion'. In this description of the magnetic field configuration we mainly observe the dynamics of the magnetic field lines, in spite of the fact that a magnetic field line remains static and it is just followed along the toroidal direction.

The system (2) is generically non-integrable, so it can be studied only by appropriate numerical methods or by using the Poincaré map associated with the transverse cross-section. In modelling phenomena related to the tokamak physics it is natural to use the Poincaré map, because the poloidal section $(S) : \zeta = \zeta_P = \mathrm{cst}$ is an ideal Poincaré section.

The Poincaré map (also called the first return map) $T : (S) \to (S), T(\psi, \theta) = (\bar{\psi}, \bar{\theta})$ is obtained by considering $(\bar{\psi}, \bar{\theta}, \zeta_P)$ the re-intersection of the magnetic field line starting from (ψ, θ, ζ_P) with (S) after a toroidal turn. In this notation ζ_P is omitted, because it is a constant. The orbit of the point (ψ_0, θ_0) is $O(\psi_0, \theta_0) = \{(\psi_0, \theta_0), (\psi_1, \theta_1), \ldots, (\psi_n, \theta_n), \ldots\}$, where $(\psi_{k+1}, \theta_{k+1}) = T(\psi_k, \theta_k)$ for all $k \in N$.

The Poincaré map describing the magnetic field lines in tokamaks must have two (independent) properties [1]: to be an area-preserving map (property imposed by the symplecticity of the Hamiltonian system) and to be compatible with the toroidal geometry (i.e. $\psi = 0 \Rightarrow \bar{\psi} = 0$—which means that the polar axis of the torus is invariant—and $\psi > 0 \Rightarrow \bar{\psi} > 0$—due to the fact that the toroidal flux $\psi = r^2/(2a^2)$ has only positive values).

In order to obtain a map which is a good approximation of the Poincaré map, one can use the powerful Hamilton–Jacobi method [10]. The first order symmetric map derived in [10] on the basis of the Hamilton–Jacobi method can be written as follows:

$$T_N : \begin{cases} \Psi_k = \psi_k - \dfrac{\partial S^{(k)}}{\partial\theta_k} \\ \Theta_k = \left(\theta_k + \dfrac{\partial S^{(k)}}{\partial\Psi_k}\right) \bmod(2\pi), \\ \bar{\Theta}_k = (\Theta_k + w(\Psi_k)(\zeta_{k+1} - \zeta_k)) \bmod(2\pi) \\ \Psi_{k+1} = \Psi_k, \\ \theta_{k+1} = \left(\bar{\Theta}_k - \dfrac{\partial S^{(k+1)}}{\partial\Psi_{k+1}}\right) \bmod(2\pi) \\ \psi_{k+1} = \Psi_{k+1} + \dfrac{\partial S^{(k+1)}}{\partial\theta_{k+1}}, \end{cases} \tag{4}$$

where $w(\psi) = 1/q(\psi)$ is the spatial frequency of the unperturbed motion and $S^{(k)} = S(\theta_k, \Psi_k)$ is the value of the generating function $G(\theta, \Psi, \zeta, \zeta_0)$ taken at section $\zeta = \zeta_k$, i.e. $S(\theta_k, \Psi_k) = G(\theta_k, \Psi_k, \zeta_k, \zeta_0)$. The first order generating

function in the finite interval $\zeta_k \leqslant \zeta \leqslant \zeta_{k+1}$ is given by the expression

$$G(\theta, \Psi, \zeta, \zeta_0) = -(\zeta - \zeta_0) \sum_{mn} H_{mn}(\Psi) \times [a(x_{mn}) \sin(m\theta - n\zeta + \chi_{mn}) + b(x_{mn}) \cos(m\theta - n\zeta + \chi_{mn})]$$

where $a(x) = [1 - \cos(x)]/x$, $b(x) = \sin(x)/x$, $x_{mn} = (m/q(\Psi) - n)(\zeta - \zeta_0)$ and χ_{mn} are phases. For the symmetric mapping the free parameter ζ_0 is taken exactly in the middle of the interval $[\zeta_k, \zeta_{k+1}]$. The sections $\zeta = \zeta_k$ are equally distanced and the mapping step is $2\pi/N = \zeta_{k+1} - \zeta_k$. The first return map is in this case

$$T = \underbrace{T_N \circ T_N \circ \cdots \circ T_N}_{N\ times}. \tag{5}$$

In the poloidal section $\zeta = 0$ the map T obeys the condition $T(\psi, 2\pi - \theta) = T(\psi, \theta)$ for all $\psi > 0$ and $\theta \in [0, 2\pi)$; hence its graph is symmetric to the lines $\theta = \pi$ and $\theta = 0$. As a consequence, the orbit of any point (ψ, θ) is symmetric to these lines. In other poloidal sections the orbits are obtained by a rotation of the orbit obtained in the section $\zeta = 0$.

3. Criteria for measuring the accuracy of a mapping model

In what follows we will not compare the results obtained using map (5) with those obtained by using the numerical integration, because this analysis has already been performed in [10] on various examples. We will compare the accuracy of map (5) obtained for different values of N and we will propose some criteria for choosing the optimal mapping step.

The strategy is the following: an indicator of the accuracy $\mathrm{IA}(N)$ and an acceptable error E are considered and the optimal step N_0 is the smallest N for which $|\mathrm{IA}(N+1) - \mathrm{IA}(N)| < E$.

In order to compute $\mathrm{IA}(N)$, we will consider p equally distanced points situated on the line $\theta = \pi$. A local indicator of the accuracy $(\mathrm{IA}_s(N), s = \overline{1, p})$ will be computed and $\mathrm{IA}(N)$ will be the average of these values, i.e. $\mathrm{IA}(N) = 1/p \sum_{s=1}^{p} \mathrm{IA}_s(N)$.

The local indicator of the accuracy can be chosen by using the following criteria.

Criterion I (the mean energy error criterion). For the orbit of n points starting from (ψ_0, θ_0) a local indicator of the accuracy is the mean energy error:

$$\mathrm{MER}(\psi_0, \theta_0) = \|H - H(\psi_0, \theta_0)\|_2^2 = \frac{1}{n} \sum_{k=1}^{n} (H(\psi_k, \theta_k) - H(\psi_0, \theta_0))^2. \tag{6}$$

This criterion uses the invariance of the Hamiltonian along the orbit and measures the deviation of the Hamiltonian on the mapped orbit from its initial value. In order to describe the local accuracy of the map, we verify the smallness of $\mathrm{MER}(\psi_0, \theta_0)$ is. The more accurate mapped orbit corresponds to the smaller value of $\mathrm{MER}(\psi_0, \theta_0)$.

Due to the fact that we suppose the Hamiltonian to be invariant along the orbit (it does not depend on ζ in our case), this criterion may be applied in a restrained number of cases (example 1 in section 4). However, it can provide useful information also in cases when the Hamiltonian is almost constant along the orbits, that is it varies only slightly, i.e. $|\mathrm{d}H/\mathrm{d}\zeta| = |\partial H/\partial \zeta| \ll 1$ (as in examples 2 and 3 studied in section 4). It can be applied to the system with a large variation only in the regions close to elliptic periodic points (inside the magnetic islands), where, due to its continuity and the specific form of the orbits, the Hamiltonian has small variations.

It should be mentioned that the symplectic integrators and the mapping based on the generating function do not always conserve the Hamiltonian along the orbit (even if it is the first integral of the system). Interesting results and comments on this topic can be found in [13], where chapter 4 is devoted to the integration methods that conserve the first integrals and chapter VI describes the symplectic integration of Hamiltonian systems, including the generating function method.

Another way to study the local accuracy of a map is to integrate the system starting from (ψ_0, θ_0) forward in time until a certain 'time' instant n, and then to integrate the system starting from (ψ_n, θ_n) backward and to verify the closeness of the forward orbit of (ψ_0, θ_0) and the backward orbit of (ψ_n, θ_n).

More precisely, the forward orbit of (ψ_0, θ_0) is $O(\psi_0, \theta_0) = \{(\psi_0, \theta_0) \ldots (\psi_n, \theta_n)\}$ and the backward orbit of (ψ_n, θ_n) is denoted by $O_{\mathrm{inv}}(\psi_n, \theta_n.) = \{(\psi'_n, \theta'_n), (\psi'_{n-1}, \theta'_{n-1}) \ldots (\psi'_0, \theta'_0)\}$.

In order to compute the distance between $O(\psi_0, \theta_0)$ and $O_{\mathrm{inv}}(\psi_n, \theta_n)$, the distance between the points $A_k(\psi_k \cdot \cos(\theta_k), \psi_k \cdot \sin(\theta_k))$ and $B_k(\psi'_{n-k} \cdot \cos(\theta'_{n-k}), \psi'_{n-k} \cdot \sin(\theta'_{n-k}))$ is used.

Here $\mathrm{dist}(k) = \left[(\psi_k \cos(\theta_k) - \psi'_{n-k} \cos(\theta'_{n-k}))^2 + (\psi_k \sin(\theta_k) - \psi'_{n-k} \sin(\theta'_{n-k}))^2\right]^{1/2}$ represents the error at the 'k' iteration.

Criterion II (the forward–backward error). For the orbit of n points starting from (ψ_0, θ_0) a local indicator of the accuracy is the forward–backward error:

$$\mathrm{FBE}(\psi_0, \theta_0) = \frac{1}{n+1} \sum_{k=0}^{n} \mathrm{dist}(k). \tag{7}$$

Theoretically the points A_k and B_{n-k} must coincide, because they are obtained by using a map and its inverse, but the accumulation of the round-off errors, automatically generated by the computer, leads to a different situation: when the point (ψ, θ) is mapped one step forward and then one step backward, a new point (ψ', θ'), close to the initial one, is obtained. A small distance between (ψ, θ) and (ψ', θ') is a sign of the good accuracy of the method. It is not always true that by decreasing the mapping step we will automatically achieve better accuracy. This happens in zones with regular dynamics (librational orbits situated inside the magnetic island or rotational orbits), but in the chaotic zones, governed by the sensitive dependence on initial conditions, decreasing the mapping step means increasing the accumulation of the round-off errors, because at each step complicated implicit equations have to be solved. This phenomenon can drastically distort the orbit.

From the previous considerations it follows that one can use the forward–backward indicator, in order to decide whether

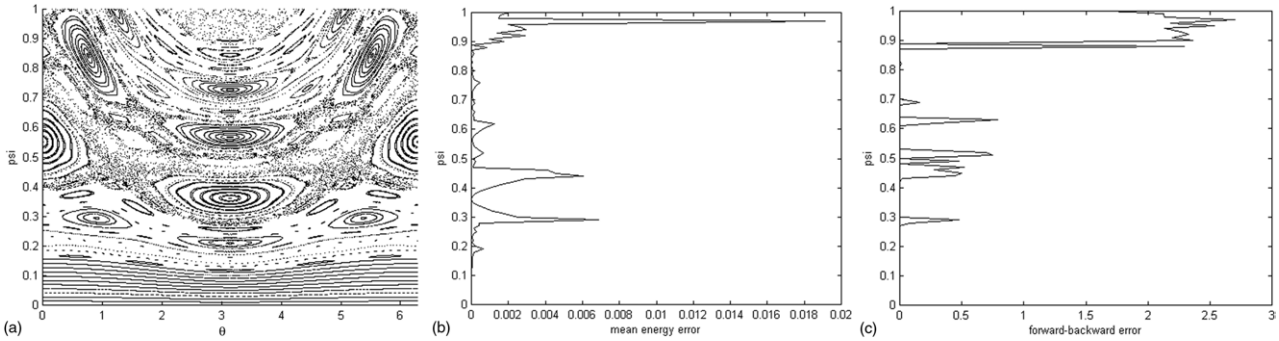

Figure 1. (*a*) The phase portrait of the HJ-tokamap corresponding to $q(0) = 1$ and $\varepsilon = 6/(4\pi^2) \approx 0.152$; (*b*) the mean energy errors of the orbit drawn in (*a*); (*c*) the forward–backward errors of the orbits drawn in (*a*).

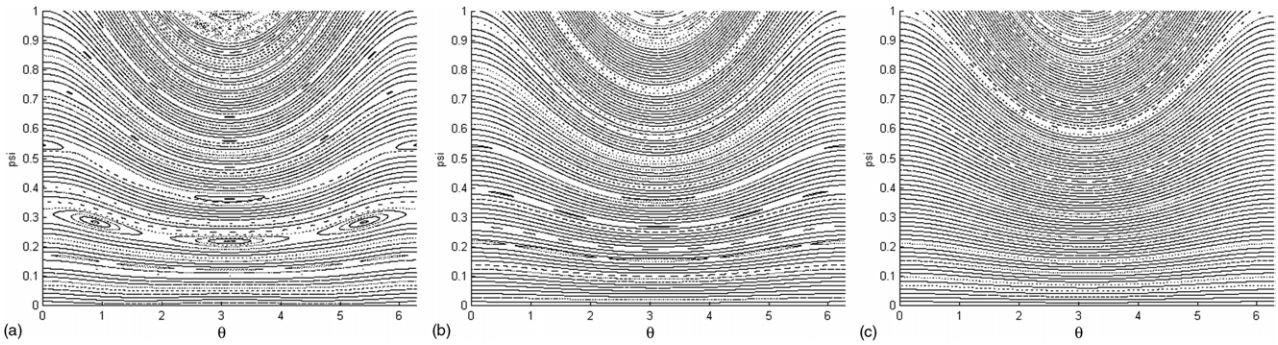

Figure 2. The phase portrait of the HJ-tokamap corresponding to $q(0) = 1$ and $\varepsilon = 6/(4\pi^2) \approx 0.152$; (*a*) for $N = 2$, (*b*) for $N = 3$, (*c*) for $N = 4$.

an orbit is regular or chaotic: a small value of FBE(ψ_0, θ_0) (less than 10^{-6}, for example) means that the orbit is regular and a large value of FBE(ψ_0, θ_0) (of order 10^{-1}, for example) means that the orbit is chaotic.

4. Applications

The criteria introduced in the previous section can be used to determine the optimal mapping step in three cases: (i) for an integrable system, (ii) for a system with a weak chaotic regime and (iii) for a system with a strong chaotic regime.

In order to obtain the mapping model, the Hamiltonian of the system is introduced in the generating function $G(\theta, \Psi, \zeta, \zeta_0)$, the map T_N for different values of N is obtained by means of (4) and finally the Poincaré map that generates the mapping model is obtained using (5).

4.1. An integrable model

The first model we will analyse was inspired by the tokamap model [6].

The Hamiltonian of the system is

$$H(\psi, \theta, \zeta) = \frac{1}{4 \cdot q(0)} \cdot \int (2 - \psi) \cdot (\psi^2 - 2\psi + 2) \mathrm{d}\psi - \varepsilon \frac{\psi}{\psi + 1} \cos\theta. \quad (8)$$

The safety factor $q(\psi) = 4 \cdot q(0)/((2 - \psi) \cdot (\psi^2 - 2\psi + 2))$ was derived in [14] by assuming that the density and electron temperature profiles in the tokamak are, respectively, $n(r) = n(0) \cdot (1 - r^2)$ and $T_e(r) = T_r(0) \cdot (1 - r^2)^2$. Because q is a monotonous increasing function, the symmetric map is a twist map. The global perturbation was considered in [6], in order to ensure the compatibility of the symmetric map with the toroidal geometry. We call the map obtained from (5) the HJ-tokamap (the Hamilton–Jacobi-tokamap).

In figures 1 and 2 we show the orbits of 100 equally spaced points situated on the line $\theta = \pi$. The orbits were obtained from (5) for $N = 1$ (figure 1(*a*)), $N = 2$ (figure 2(*a*)), $N = 3$ (figure 2(*b*)) and $N = 4$ (figure 2(*c*)). In the Hamiltonian we considered $q(0) = 1$ and $\varepsilon = 6/(4\pi^2) \approx 0.152$.

Hamiltonian (8) is conserved along the trajectories, because it does not explicitly depend on ζ, which means that the system is integrable and all the orbits are regular. Due to this specific property, an intuitive determination of the mapping step can be proposed by analysing the phase portraits obtained for different N.

In figure 1(*a*), corresponding to $N = 1$, some large chaotic zones can be observed. It means that the mapping step $2\pi/1$ is too large for a correct description and that the stochasticity has been artificially created. In figure 2(*a*), corresponding to $N = 2$, it is seen that the island chains of type (3, 2) and (2, 1) have relatively large widths and thin chaotic layers surround the hyperbolic periodic points, even if they cannot be observed in the phase portrait. This means that the mapping step $2\pi/2$ is also too large for a correct description. Due to the fact that the main island chains are very thin in figure 2(*b*), corresponding to $N = 3$, and that they are practically not seen in figure 2(*c*), corresponding to $N = 4$, we may intuitively conclude the mapping step $2\pi/3$ is convenient, but $2\pi/4$ is appropriate

Table 1.

	$N=1$	$N=2$	$N=3$	$N=4$	$N=5$
MER(N)	0.0009	0.000 02	0.000 0009	0.000 0002	0.000 000 08
FBE(N)	0.32	0.12	0.013	0.000 006	0.000 004

for an accurate description of the continuous system. This assertion will be verified by using the criteria presented in section 3.

In order to use Criterion I, the mean energy error of each orbit was computed using (6).

In figure 1(b) we show the mean energy errors corresponding to the orbits presented in figure 1(a), obtained for $N = 1$. It can be seen that the local maxima of the mean energy errors correspond to 'artificial' chaotic orbits: the chaotic layer surrounding the island chains of type (3, 2), (5, 3) (2, 1) and the chaotic orbits with a large radial excursion, i.e. for $\psi > 0.89$.

The global mean energy errors, MER(N), presented in table 1 were obtained by averaging the mean energy errors of the orbits previously analysed.

By using the procedure described in section 3, the following results were obtained:

- if the admissible error is $E = 10^{-4}$, then the optimal step is $2\pi/2$, corresponding to $N = 2$.
- if the admissible error is $E = 10^{-6}$, then the optimal step is $2\pi/3$, corresponding to $N = 3$.
- if the admissible error is $E = 5 \times 10^{-7}$, then the optimal step is $2\pi/4$, corresponding to $N = 4$.

Criterion II can also be useful for the study of the accuracy of a mapping model.

The forward–backward errors of the orbits presented in figure 1(a), each containing 1000 points, are shown in figure 1(c). As expected from theoretical considerations, the local maxima of the forward–backward error are obtained (artificially created) for chaotic orbits. This effect is due to the sensitive dependence on initial conditions. Because the chaotic orbits surrounding the island chains of type (3, 2), (5, 3), (2, 1) live in a bounded region, these maxima are relatively small. However a large variation can be observed for $\psi > 0.89$, i.e. for the chaotic orbits with a large radial excursion.

The forward-backward errors, FBE(N), presented in Table 1 were obtained by averaging the forward–backward errors of the orbits.

The values of FBE(1) and FBE(2) are large due to the unbounded chaotic orbits (see figures 1(a) and 2(a)). For $N = 3$ the number of these orbits is reduced and they practically disappear for $N = 4$ and $N = 5$; hence the forward–backward errors become very small.

Because FBE(3) − FBE(4) $\approx$ 0.013 and FBE(4) − FBE(5) $\approx$ 0.000002 we may assume that an appropriate step for the study of the system is $2\pi/4$, corresponding to the admissible error $E = 10^{-5}$.

Finally it should be emphasized that the criteria which we used are independent and there is no relation between the admissible errors considered for each criterion.

The system we focused on, an integrable one, is very simple. The study was performed to verify that the criteria proposed in section 3 are realistic. But what happens in the case of non-integrable systems?

The non-integrable system which we investigate in what follows is a particular case of mapping models proposed in [15] for the study of the magnetic field lines in ASDEX-Upgrade tokamak.

4.2. A system in a weak chaotic regime

These phenomenological models rely heavily on experimental data obtained on the ASDEX-Upgrade tokamak.

The safety factor, $q(\psi) = 0.8{+}4\psi$, correctly describes the experimental position of the MHD modes in ASDEX-Upgrade and the perturbations

$$H_{m,n} = \rho_{m,n} \cdot \begin{cases} \alpha \left(\dfrac{\psi}{\psi_{m,n}}\right)^{m/2} \left[1 - \beta \left(\dfrac{\psi}{\psi_{m,n}}\right)^{1/2}\right], \\ \psi \leqslant \psi_{mn}, \\ \dfrac{\alpha(1-\beta)-\gamma+\gamma\left(\dfrac{\psi}{\psi_{mn}}\right)^{1/2}}{\left(\dfrac{\psi}{\psi_{mn}}\right)^{(m+1)/2}}, \\ \psi > \psi_{mn}, \end{cases} \tag{9}$$

were deduced from ECE measurements.

The Hamiltonian of the system is

$$H(\psi, \theta, \zeta) = H_0(\psi) + H_1(\psi, \theta, \zeta) = \frac{\ln(0.8 + 4\psi)}{4} + \sum_{m,n} H_{m,n}(\psi) \cdot \cos(m\theta - n\zeta). \tag{10}$$

It our study we will consider$\alpha = 0.04$, $\beta = 0.87$, $\gamma = 0.005$, values derived from the experiment.

The radial positions of the(3, 2), (4, 3) and (1, 1) NTM in the ideal system are $\psi_{3,2} = 0.175$, $\psi_{4,3} = 0.133$ and $\psi_{1,1} = 0.05$.

Because the (3, 2) and (1, 1) modes are separated by quite a large distance ($\psi_{3,2} - \psi_{1,1} = 0.125$), they do not overlap for moderate values of the perturbations amplitudes. If they are locked together they generate a (non-integrable) system with a weak chaotic regime, in the sense that the chaotic zones surrounding the (3, 2) mode, respectively, the (1, 1) mode, are thin layers that do not intersect. The influence of the dynamics of a particular mode on the dynamics of other modes is small.

In this case the Hamiltonian of the system is

$$H(\psi, \theta, \zeta) = H_0(\psi) + H_1(\psi, \theta, \zeta) = \frac{\ln(0.8 + 4\psi)}{4} + H_{3,2}(\psi) \cdot \cos(3\theta - 2\zeta) + H_{1,1}(\psi) \cdot \cos(\theta - \zeta). \tag{11}$$

We call the map generated by the Hamiltonian (11) the WCR-ASDEX map (a weak chaotic regime ASDEX map).

We are interested whether these chaotic zones are determined by some intrinsic properties of the system or whether they are generated by numerical imperfections in the discrete model, as in the previous example for the mapping step 2π.

The amplitudes of the Hamiltonian perturbations are $\rho_{3,2} = 0.0875$ and $\rho_{1,1} = 0.0475$.

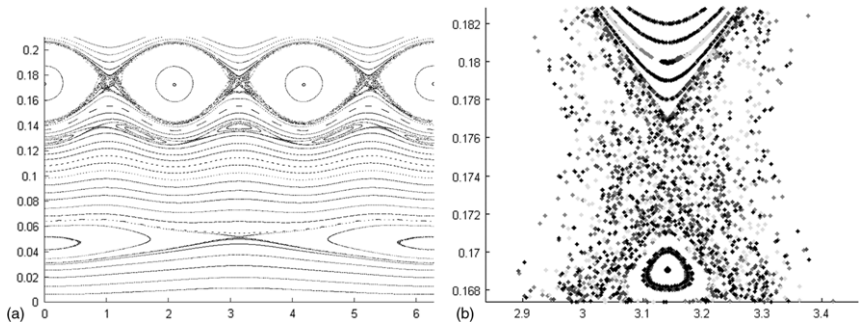

Figure 3. (*a*) Phase portrait of the WCR-ASDEX map corresponding to $\alpha = 0.04$, $\beta = 0.87$, $\gamma = 0.005$, $\rho_{3,2} = 0.0875$ and $\rho_{1,1} = 0.0475$, obtained for $N = 1$; (*b*) part of the phase portrait.

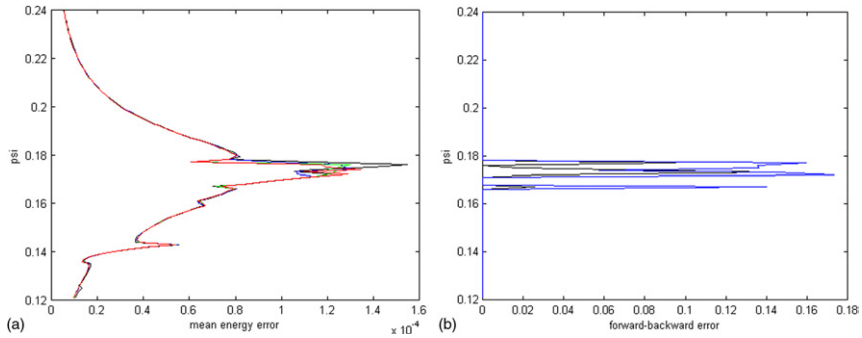

Figure 4. The WCR-ASDEX corresponding to $\alpha = 0.04$, $\beta = 0.87$, $\gamma = 0.005$, $\rho_{3,2} = 0.0875$ and $\rho_{1,1} = 0.0475$: (*a*) the local mean energy error (*b*) the forward–backward error.

The phase portrait presented in figure 3(*a*) illustrates the previous considerations. It was obtained using (5) with $N = 1$, but similar figures can also be obtained for $N = 2$, $N = 3$ and $N = 4$. A part of the phase portrait, the region situated near the (3, 2) hyperbolic point on the line $\theta = \pi$, is shown in figure 3(*b*). (The black points correspond to the mapping step $2\pi/1$, the blue points to $2\pi/2$, the green points to $2\pi/3$ and the red points to $2\pi/4$.) It can be seen that the regular orbits practically coincide for all considered values of N and that the chaotic layer is not smaller for larger N. From these figures we intuitively conclude that the weak chaos is a property of the system and that there are no important differences between the mapping models obtained for $N \in \{1, 2, 3, 4\}$.

For a rigorous study we use the criteria introduced in section 3. We focus on the annulus $0.12 \leqslant \psi \leqslant 0.24$, because the (3, 2) mode is situated in this region. In order to capture the main dynamical properties of the system, we analysed 120 orbits starting from equally separated points on the line $\theta = \pi$. Here 5000 iterations have been done.

In this case the Hamiltonian is not constant along the orbit. However, because it has a small variation ($|\mathrm{d}H/\mathrm{d}\zeta| = |\partial H/\partial\zeta| < 0.0017$ for all orbits), the information provided by the mean energy criterion can be useful.

The mean energy errors for these orbits are presented in figure 4(*a*) (black points for $N = 1$, blue points for $N = 2$, green points for $N = 3$ and red points for $N = 4$). The fact that the orbits corresponding to different N coincide can be deduced from the quasi-coincidence of the mean energy error curves.

Table 2.

	$N = 1$	$N = 2$	$N = 3$	$N = 4$
MER(N)	0.000 0394	0.000 0387	0.000 0386	0.000 0385
FBE(N)	0.0033	0.0079	0.0074	0.0073

The largest values of the mean energy error are obtained for $\psi \approx 0.175$, i.e. near the hyperbolic periodic point and they are the sign of the presence of chaos.

The values of the global mean energy errors are given in table 2.

Using the method described in section 3, we can deduce the optimal mapping step for a prescribed admissible error:

- for an admissible error $E = 10^{-5}$ the optimal step is obtained with $N = 1$,
- for an admissible error $E = 10^{-6}$ the optimal step is obtained with $N = 2$.

In order to use the forward–backward error as an indicator of the accuracy of the mapping model, the local forward–backward errors of the 120 orbits considered above were computed. The results are plotted in figure 4(*b*). One can see a large peak in the same region where the large values of the mean energy error are situated. This indicates that there are chaotic orbits, due to the sensitive dependence on initial conditions.

The values of the global forward-backward errors (table 2) point to an interesting and unexpected situation: the error corresponding to $N = 2$, i.e. FBE(2) = 0.0079, is larger

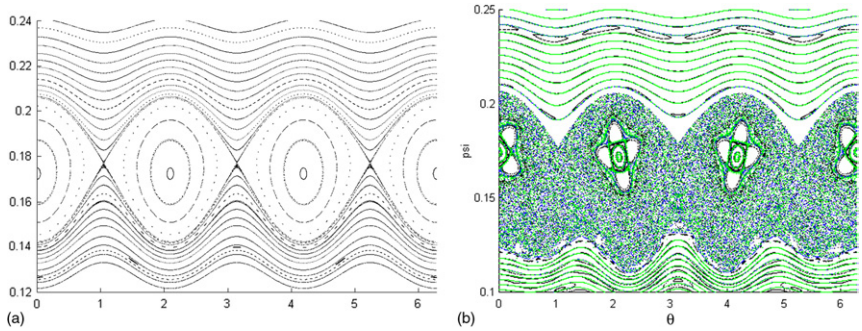

Figure 5. (*a*) Phase portrait of the SCR-ASDEX map, $\rho_{3,2} = 0.0875$, $\rho_{4,3} = 0$, $N = 1$. (*b*) Phase portrait of the SCR-ASDEX map, $\rho_{3,2} = 0.0875$, $\rho_{4,3} = 0.0428$, $N = 1$.

than the error obtained for $N = 1$ and the values comparable to FBE(2) are obtained for $N = 3$ and $N = 4$.

This means that the chaotic zone surrounding the hyperbolic points is slightly larger in the models obtained for $N \in \{2, 3, 4\}$ than in the model obtained for $N = 1$. This phenomenon is confirmed by figure 4(*b*). The explanation can be the following: by modifying the mapping step the orbits situated near the boundary of the chaotic zone are affected because of accumulation of the round-off errors, some regular orbits are pushed in the chaotic zone and remain there.

The optimal mapping step is obtained by applying the procedure described in section 3:

- for the admissible error $E = 10^{-2}$ the optimal step is obtained for $N = 1$,
- for the admissible error $E = 10^{-3}$ the optimal step is obtained for $N = 2$.

Thus, in this case the chaotic area is slightly enlarged by decreasing the mapping step until the process is stabilized.

4.3. A system in a strong chaotic regime

In order to obtain a model in a strong chaotic regime we will consider the perturbations corresponding to the (3,2) and (4,3) NTM in Hamiltonian (10). In the unperturbed case these modes are located on the lines $\psi_{3,2} = 0.175$, respectively, $\psi_{4,3} = 0.133$. They are relatively close to each other. Therefore for moderate perturbation amplitudes the modes will overlap producing a large chaotic zone around them. We call this a strong chaotic regime.

The Hamiltonian of the system is

$$H(\psi, \theta, \zeta) = H_0(\psi) + H_1(\psi, \theta, \zeta) = \frac{\ln(0.8 + 4\psi)}{4} + H_{3,2}(\psi) \cdot \cos(3\theta - 2\zeta) + H_{4,3}(\psi) \cdot \cos(4\theta - 3\zeta). \tag{12}$$

The map obtained with (4) and (5) using Hamiltonian (12) will be called strong chaotic regime in ASDEX (SCR-ASDEX).

In figure 5(*a*) we show the phase portrait of the map for which only the (3,2) mode was activated, i.e. $\rho_{3,2} = 0.0875$ and $\rho_{4,3} = 0$, obtained with (5) for $N = 1$. The width of the islands surrounding the elliptic points is large due to the relatively large value of the perturbation amplitude $\rho_{3,2}$. The (4, 3) mode can be seen in the lower part of the figure. Figure 5(*b*) shows the phase portrait of the SCR-ASDEX map when the (3, 2) and (4, 3) modes are locked together. Here $N = 1$ (black points), $N = 2$ (blue points) and $N = 3$ (red points). The perturbation amplitudes are $\rho_{3,2} = 0.0875$ and $\rho_{4,3} = 0.0428$. A large chaotic zone surrounding the two modes arises because they overlap. However the zone is practically the same for all values of N. In the upper part of figure 5(*b*) in the phase portrait obtained for $N = 1$ (black points) an island chain can be seen. It is reduced to a rotational orbit in the phase portrait obtained for $N = 2$ and $N = 3$.

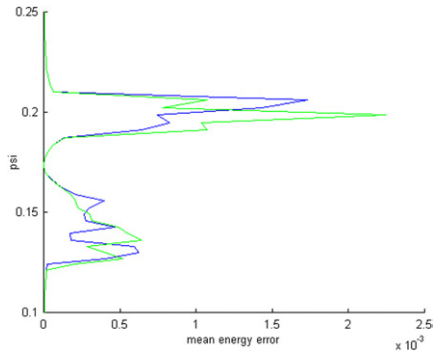

Figure 6. The local mean energy errors for the SCR-ASDEX map, $\rho_{3,2} = 0.0875$, $\rho_{4,3} = 0.0428$, and $N = 2$ (blue line), $N = 3$ (green line).

The Hamiltonian is not constant along the orbits. However, its variation is rather small ($|\mathrm{d}H/\mathrm{d}\zeta| = |\partial H/\partial\zeta| < 0.0019$ for all orbits). In this case the information provided by the mean energy criterion can be useful.

In order to compute the mean energy error, we choose 165 orbits starting from the points situated on the line $\theta = 0$ from $\psi = 0$ to $\psi = 0.5$. The local mean energy error of these orbits is plotted in figure 6, for $N = 2$ (blue line) and $N = 3$ (green line).

Rather large values of the local mean energy error are observed in the chaotic zone $0.13 < \psi < 0.18$, which is natural, and near $\psi = 0.2$ where the orbits are regular but have a strongly curved shape.

The values of the global mean energy error are given in table 3:

- for the admissible error $E = 10^{-5}$ the optimal step is 2π obtained for $N = 1$,
- for the admissible error $E = 10^{-6}$ the optimal step is π obtained for $N = 2$.

Table 3.

	$N = 1$	$N = 2$	$N = 3$
MER(N)	0.000 0072	0.000 0061	0.000 0068
FBE(N)	0.000 035	0.000 033	0.000 034

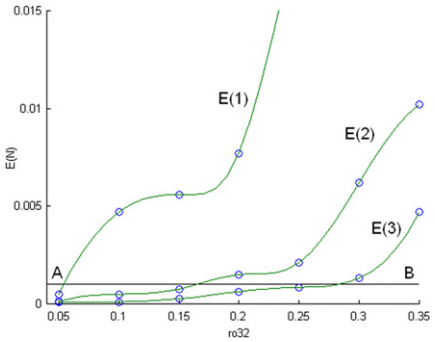

Figure 7. The values of $E(1)$, $E(2)$ and $E(3)$ for $\rho_{3,2} \in [0.05, 0.35]$.

The values of the global forward–backward errors obtained for $N \in \{1, 2, 3\}$ are much closer.

For an admissible error $E = 10^{-5}$ the optimal step is 2π.

In this case the mapping model with the step 2π provides a sufficiently accurate discretization of the considered Hamiltonian system. The chaotic dynamics in this case is an intrinsic property of the system.

4.4. The dependence of the optimal mapping step on the strength of the perturbation amplitude

We focus on the optimal mapping steps obtained by using the forward–backward error criterion, because we are mainly interested in the study of non-integrable systems.

In order to investigate the influence of the perturbation amplitude on the optimal mapping step, we consider the WCR-ASDEX map defined in section 4.2. The perturbation amplitude of the $(1, 1)$ mode is fixed, $\rho_{1,1} = 0.0475$, but the perturbation amplitude of the $(3, 2)$ mode is varied in the interval $[0.05, 0.35]$.

The indicator of accuracy FBE(N) is obtained by using 120 orbits starting from equally spaced points situated on the line $\theta = \pi$ in the region $0.12 \leqslant \psi \leqslant 0.24$. Here each orbit contains 5000 points.

The admissible error considered in this analysis is $E = 10^{-3}$.

In figure 7 we show the values of $E(N) = |\mathrm{FBE}(N + 1) - \mathrm{FBE}(N)|$ for $N \in \{1, 2, 3\}$ and $\rho_{3,2} \in [0.05, 0.35]$. The values corresponding to $\rho_{3,2} = 0.05 \cdot k$, $k = \overline{1, 7}$ (small circles in the figure) were interpolated by using the cubic spline technique. The horizontal line AB corresponds to the admissible error $E = 10^{-3}$.

The optimal mapping step is $2\pi/N$, where N is the smallest natural number that satisfies the condition $E(N) \leqslant E$, i.e. the graph of $E(N)$ is situated below the line AB.

From the method presented in section 3 it follows that

- for $\rho_{3,2} \in [0, 0.054]$ the optimal mapping step is 2π, corresponding to $N = 1$,
- for $\rho_{3,2} \in (0.054, 0.165]$ the optimal mapping step is $2\pi/2$, corresponding to $N = 2$,
- for $\rho_{3,2} \in (0.165, 0.284]$ the optimal mapping step is $2\pi/3$, corresponding to $N = 3$.

Thus, in order to obtain the same accuracy of the model, we must decrease the mapping step, when the perturbation amplitude increases.

5. Conclusions

The main objective of this paper is connected with the optimal discretization of continuous dynamical systems. More precisely the work was focused on the study of the accuracy of the mapping models obtained from Hamiltonian systems by using the Hamilton–Jacobi method. Instead of the indicators of numerical accuracy (usually this is the magnitude of the largest neglected term in an expansion in series), we used some 'dynamical' indicators (the mean energy error and the forward–backward error), specific for this type of models. The mean error allows us to determine rather clearly the optimal mapping step for integrable systems. It is also useful for quasi-stationary systems. This criterion correlates the mapping step which has to be chosen with the imposed admissible error. The second accuracy criterion uses as an indicator the forward–backward error and it is very useful in the study of chaotic systems. The criterion makes it possible to optimally choose the mapping step in such a way that the chaos introduced by the numerical computation (the numerical chaos) can be neglected when compared with the intrinsic chaotic behaviour.

The two global criteria of accuracy were used for determining the optimal mapping step in three situations: (i) an integrable model, when the criteria were used only for proving that they are realistic, (ii) a system with a weak chaotic regime and (iii) a system with a strong chaotic regime.

For a future work one could think about more sophisticated indicators for choosing the optimal mapping step in the cases with chaotic regimes. Here the corresponding time series in principle contain two components of chaos: intrinsic and artificial due to insufficient accuracy of the mapping. By analysing the Fourier spectra of the series obtained for different values of N it should be possible to separate the two components and to draw some conclusions about the optimal mapping step.

Acknowledgments

Helpful discussions with S.S. Abdullaev, R. Balescu and K. Spatschek on various aspects of mappings and their applications are acknowledged.

References

[1] Balescu R. 1988 *Transport Processes in Plasmas* (Amsterdam: Elsevier/North-Holland)
[2] Martin T.J. and Taylor J.B. 1984 *Plasma Phys. Control. Fusion* **26** 321
[3] Wobig H. 1987 *Z. Naturf. Teil* A **42** 1054
[4] Punjabi A., Verma A. and Boozer A. 1992 *Phys. Rev. Lett.* **69** 3392

[5] Abdullaev S.S. and Zaslavski G.M. 1995 *Phys. Plasmas* **2** 4533
[6] Balescu R., Vlad M. and Spineanu F. 1998 *Phys. Rev.* E **58** 951
[7] Davidson M.G., Dewar R.L., Gardner H.J. and Howard J. 1995 *Aust. J. Phys.* **48** 871
[8] Oda G.A. and Caldas I.L. 1995 *Chaos, Solitons Fractals* **5** 15
[9] Balescu R. 1998 *Phys. Rev.* E **58** 3781
[10] Abdullaev S.S. 2002 *J. Phys. A: Math. Gen.* **35** 2811
[11] Abdullaev S.S. 2004 *Nucl. Fusion* **44** S12
[12] Abdullaev S.S. 2006 *Construction of Mappings for Hamiltonian Systems and their Applications* (*Lecture Notes in Physics* vol 691) (Berlin: Springer)
[13] Hairer E., Lubich C. and Wanner G. 2002 *Geometric Numerical Integration, Structure-Preserving Algorithms for Ordinary Differential Equations* (Berlin: Springer)
[14] Misguich J.H. *et al* 2003 *Ann. Physique.* **28** 1–101
[15] Igochine V., Dumbrajs O., Constantinescu D., Zohm Z., Zvejnieks G. and ASDEX Upgrade Team 2006 *Nucl. Fusion* **46** 741